

Pulsating red giant stars

Ensemble asteroseismology and Asteroseismology of stellar populations in the Milky way

B. Mosser¹ and A. Miglio²

¹ LESIA, Observatoire de Paris, PSL Research University, CNRS, Université Pierre et Marie Curie, Université Paris Diderot, 92195 Meudon, France

² School of Physics and Astronomy, University of Birmingham, Edgbaston, Birmingham, B15 2TT, UK

1. Introduction

Asteroseismology of low-mass stars has provided us with a much more precise method for determining stellar global parameters than classical methods such as isochrone fitting (e.g. [Lebreton & Goupil 2014](#)). The determination of accurate stellar parameters is a fundamental and longstanding problem in astrophysics (e.g. [Soderblom 2010](#)). Nevertheless, such a determination is only possible by means of stellar models and therefore suffers from our deficient knowledge of the physical processes taking place in stars. It motivated the development of a new field called ensemble asteroseismology as described thoroughly in Sect. 2. The wealth of red giants observed by CoRoT as well as the knowledge of their oscillation spectra (Sect. 2.2) made it possible to adopt a statistical approach. The foundations of such an approach are the relations between global seismic quantities, such as the large separation or the frequency of the maximum height of the power spectrum, and stellar parameters. Initially, these scaling relations were used to predict the characteristics of the oscillations (e.g. [Ulrich 1986](#); [Brown et al. 1991](#)). CoRoT permitted to go beyond by using the scaling relations for unraveling the structure and evolution of low-mass red giant stars (Sect. 2.3).

Such a wealth of seismic indices also allowed the development of a novel approach for investigating the Galactic stellar populations (Sect. 3). For instance, the global seismic constraints have been used for inferring accurate distances as well as an estimate of the red giant ages. All this information brings new lights for investigating stellar populations in the Milky Way. A step further is also permitted by the opportunity gathered by the synergies between asteroseismology and large spectroscopic surveys (Sect. 3.2), which

is ending up with the emergence of a chemodynamical investigation of the Galaxy.

2. Ensemble asteroseismology (by B. Mosser)

Before the launch of CoRoT, asteroseismic observations were limited to a handful of targets. With high-precision radial velocity measurement, observations could be performed on one single object only at the same time. A six-week photometric campaign using nine telescopes allowed the simultaneous monitoring of about 20 red giants in the open cluster M67 ([Stello et al. 2007](#)). CoRoT, offering the possibility to observe simultaneously and continuously thousands of targets and to derive their seismic properties, has promoted a new concept: ensemble asteroseismology. This concept is developed in this chapter: the measurement of global seismic parameters allows us to examine the properties of large populations of stars at different evolutionary stages.

2.1. The situation before CoRoT: the case of red giants

The power of seismology, as illustrated by Earth seismology and helioseismology (e.g., [Tong & Garcia 2015](#)), has motivated attempts for detecting solar-like oscillations in red giants as well as in less-evolved stars having an external convective layer (e.g., [Gilliland et al. 1993](#)). Here, we show the difficulties observations had to face for detecting solar-like oscillations in red giants and the progress they permitted. We do not address large-amplitude oscillations in semi-regular variable or Mira stars, but restrict our attention to red giants.

2.1.1. Ambiguous and unambiguous identifications

The first unambiguous detection of solar-like oscillations of a red giant star was reported by [Frandsen et al. \(2002\)](#). They monitored the G7III red giant ξ Hya during one month with the CORALIE spectrometer at the 1.2-m Swiss Euler telescope. Oscillations were identified in the frequency range 50–130 μHz , with amplitudes slightly smaller than 2 m.s^{-1} . The consensus resulted from the combination of different positive signatures, which are all related to global properties that prefigured the bases of ensemble asteroseismology. Other observations were inconclusive in terms of seismic analysis but participated to the movement toward positive detections (e.g., [Kallinger et al. 2005](#); [Kim et al. 2006](#); [Stello et al. 2007](#)). According to the current knowledge about solar-like oscillations, earlier results can be a posteriori confirmed or disconfirmed, using global properties from what is now called ensemble asteroseismology (Sect. 2.3).

2.1.2. The case of ε Ophiuchi

As Procyon for less-evolved stars (e.g., [Arentoft et al. 2008](#); [Bedding et al. 2010](#), and references therein), the G9.5III red giant ε Oph has played an important role as it was supposed to be a favorable target. [Barban et al. \(2004\)](#) reported the results of a two-month bi-site ground-based campaign, with unambiguous detection of solar-oscillation in the red giants ε Oph and η Ser. The frequency ν_{max} of maximum oscillation signal was clearly identified, contrary to the large separation $\Delta\nu$. A deeper analysis of ε Oph was then performed by [De Ridder et al. \(2006\)](#), who could measure the frequency ν_{max} of maximum oscillation, but still hesitated between two values of the large separation, which are each-other day aliases (4.8 or 6.7 μHz). These observations largely benefitted from the high stability and accuracy of high-resolution spectrometers designed for exoplanetary search. With the space-borne MOST data, oscillations around 60 μHz were confirmed ([Barban et al. 2007](#)), with maximum amplitudes around 130 ppm and a large separation of $5.3 \pm 0.1 \mu\text{Hz}$. The authors derived a mass of about $2 M_{\odot}$, assuming that the observed modes are radial. The identification of non-radial modes remained however debated. With a reanalysis of the MOST data, [Kallinger et al. \(2008a\)](#) found that the best model fit both radial and nonradial modes. The small scatter of the frequencies indicated then, against previous analysis, that the lifetimes of the modes could be as long as 10–20 days. [Mazumdar et al. \(2009\)](#) reanalyzed the data and tested if the star is burning hydrogen in a shell on the red giant branch (RGB) or is burning helium in the core. The radius they derived from the asteroseismic analysis matches the interferometric value quite closely. They found a mass of $1.85 \pm 0.05 M_{\odot}$ but could not fix the evolutionary status.¹

2.1.3. Mode lifetimes? Non-radial modes?

The case study of ε Oph showed that many issues were debated, among which the mode lifetimes and the presence of

¹ From the statistical point of view gained with the CoRoT and Kepler observations, ε Oph is likely a secondary-clump star.

non-radial modes. [Stello et al. \(2006\)](#) revisited lifetimes in the oscillation spectrum of ξ Hya and concluded that the data are consistent with mode lifetimes of 2 days. The re-analysis of the oscillation spectrum of ε Oph allowed two interpretations: only short-lived radial modes ([Barban et al. 2007](#)) or a mix of radial and nonradial modes with moderate lifetimes ([Kallinger et al. 2008a](#)).

In fact, observations of the K1.5 red giant Arcturus were more conclusive. [Retter et al. \(2003\)](#) showed that its amplitude spectrum observed with the star tracker on WIRE has a significant excess of power at low frequency. The variability of Arcturus was presumably explained by sound waves, the contribution of granulation only being likely ruled out by Doppler observations conducted earlier. A further analysis by [Tarrant et al. \(2007\)](#) based on a 2.5-yr long photometric time series by the SME imager on board the Coriolis satellite provided the measurement of the damping time, which was quite long (24 ± 1 days). Their results also hinted at the possible presence of non-radial modes.

[Hekker et al. \(2006\)](#) argued that the line profile variations in three stars (among which ε Oph) already analyzed with other tools suggest the presence of non-radial modes. [Kallinger et al. \(2008b\)](#) reported the detection of non-radial modes in MOST photometry of the red giant HD 20884, but this result was presented by the Editor as “an important and controversial topic”.²

2.1.4. Empirical and theoretical predictions

For all these observations, global seismic properties and scaling relations were used to guide the analysis: the large separation was scaled to the inverse of the dynamical time, proportional to the square root of the mean density ([Eddington 1917](#)); the frequency ν_{max} was scaled to the atmospheric cutoff frequency ([Brown et al. 1991](#)). The empirical scaling relations of [Kjeldsen & Bedding \(1995\)](#) were successfully used for estimating the expected frequency range and amplitudes. [Stello et al. \(2008\)](#) presented the analysis of eleven giants observed with the WIRE satellite and reported the first confirmation that ν_{max} can be predicted for K giants by scaling from the solar acoustic cutoff frequency. They used such an approach to provide an estimate of the stellar masses, and claimed a precision level of about 20%. Theoretical work could not decide if radial and non-radial modes were equally excited. [Dziembowski et al. \(2001\)](#) predicted that, for red giants, non-radial mode amplitudes should be lower than radial mode amplitudes. No reliable information was available for lifetimes.

2.1.5. Practical limitations before CoRoT

A necessary ingredient for successful seismic observations is long duration, especially for red giants that oscillate at low frequency due to their low mean density. Before CoRoT, ground-based Doppler observations reached excellent performance with high signal-to-noise ratio (Fig. IV.2.1) but

² Having demonstrated that combining different epoch observations of red giants is feasible, [Kallinger et al. \(2012\)](#) clearly showed that non-radial modes were present in ε Oph; this conclusion has been possible only after the CoRoT observations.

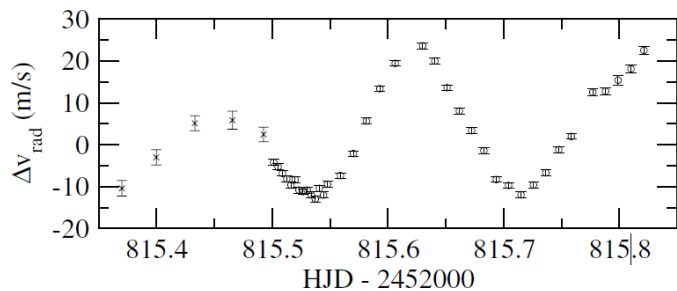


Fig. IV.2.1. Doppler time series showing the oscillations in the red giant ϵ Oph, observed with CORALIE (circles) and ELODIE (crosses), illustrating that the sensitivity is not an issue (from De Ridder et al. 2006) © A&A.

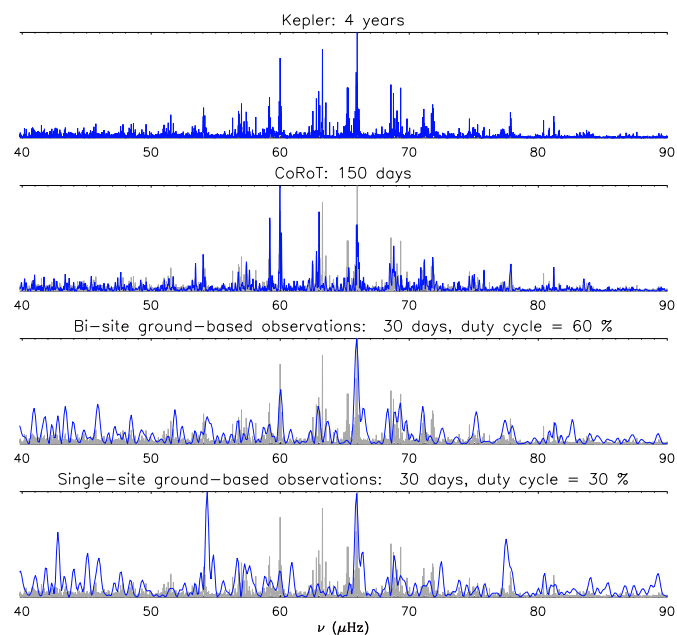


Fig. IV.2.2. Simulation of the oscillation spectrum of a $1.3-M_{\odot}$ star on the RGB, as observed with Kepler, CoRoT, or ground-based observations. In all panels, the 4-year long spectrum is indicated in grey as a reference. The noise level is supposed to be similar in all graphs.

remained affected by the day aliases and provided controversial measurements.³

The large success of CoRoT comes from the ability to observe thousands of red giants continuously for months, and the surpassing quality of Kepler comes from even longer observation capability. This is illustrated on Fig. IV.2.2, which shows how a clear oscillation signal in a typical red-clump star observed by CoRoT or Kepler is unclear with short observation duration and single or bi-site observations. When the observation conditions are degraded, the equidistance between modes disappears, distinguishing radial and non-radial modes is impossible, and measuring the life time is illusory since the frequency resolution is too poor.

³ Before the space mission MOST, ground-based seismic photometric observations remained limited to a specific case (M67) and could not be made with dedicated photometers. Star trackers onboard the HST and WIRE were not designed for satisfying the extremely demanding specifications for seismology.

2.2. Toward ensemble asteroseismology

2.2.1. The CoRoT red giant revolution

Everyone agrees that red giant asteroseismology is one of the greatest success of CoRoT and Kepler. This success however started in unfavorable conditions, since red giants represent hostile harbors for exoplanets. If we consider a typical red clump star with a radius about $10 R_{\odot}$, a planetary transit will be a hundred time dimmer than around a main-sequence star, whereas hot Jupiters do not provide any transit since their orbit is engulfed in the stellar envelope. As a consequence, red giants were first discarded from the preferred target list. They were however observed in the faint field LRc01, so that De Ridder et al. (2009) could report:

- the presence of radial and non-radial oscillations,
- for more than 300 red giant stars;
- mode lifetimes of the order of a month.

So, the main questions raised by previous observations were unambiguously answered by this pioneering work. One important feature of the red giant oscillation spectrum remained however hidden at that time: mixed modes were not identified, despite the fact they are present, as in the spectrum of the red giant CID 101600807; according to Fig. 4 of De Ridder et al. (2009), this is a star belonging to the secondary clump. Such an evidence is only a posteriori obvious, when the story is well known.

2.2.2. Structure of the oscillation spectrum

Following this firework, the harvest could start. Hekker et al. (2009) aimed at understanding the distribution of the frequencies ν_{\max} of maximum oscillation power and searched for a possible correlation between ν_{\max} and the large separation $\Delta\nu$. They determined the first properties of the background signal and the oscillation signal. Indeed, these properties are the different signatures of the convection that breaks just below the photosphere (e.g., Mathur et al. 2011; Mosser et al. 2012a; Samadi et al. 2013), with an incoherent signature that gives raise to the different scales and granulation, whereas the excited waves filtered by the star give raise to the oscillation modes.

An important leap forward was proposed by Kallinger et al. (2010), who depicted the properties of selected targets, performed grid modelling, and deduced reliable estimates for the stellar mass and radius from scaling relations (see Sect. 2.3). Mosser et al. (2010) extended the analysis toward a larger set of stars in the CoRoT fields LRc01 and LRa01, characterized according to their location in a color-magnitude diagram, with J–K in the range [0.6, 1.0] and K brighter than 12. They identified more than 1800 red giants showing solar-like oscillations among 4600 light curves and obtained accurate distributions of the stellar parameters for about 930 stars. Such global analysis on large sets of stars has opened the way to ensemble asteroseismology, with reliable estimates of mass and radius for several hundred red giants as well as precise information about the stellar population distribution and the red clump.

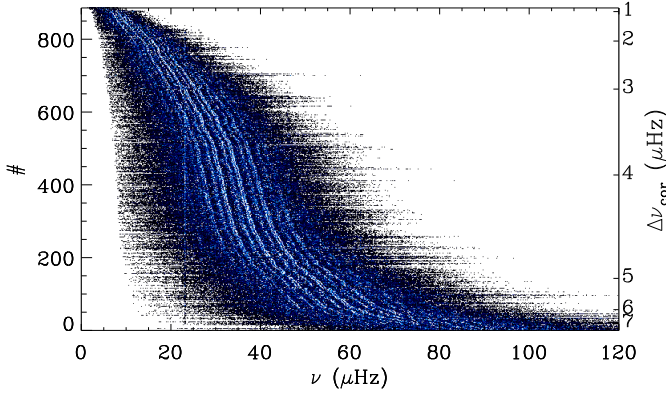


Fig. IV.2.3. CoRoT red giant power spectra stacked into an image after sorting on the large separation. Each line corresponds to one star. The sorting takes the red universal oscillation pattern into account and reveals the structure common to all red giants. The vertical line at $23.2 \mu\text{Hz}$ is the signature of the low-Earth orbit (Auvergne et al. 2009). Figure from Mosser et al. (2011b) © A&A.

2.2.3. Structure homology and universal oscillation pattern

CoRoT observations have shown a simple and useful property of the red giant oscillation pattern: following the interior structure homology, the oscillation pattern has also homologous properties. Structure homology is induced by generic physics: the thermodynamical conditions of the hydrogen-burning shell are related on the one side with the helium core, and on the other side with the convective envelope, so that the core and envelope properties are closely linked together (e.g., Kippenhahn & Weigert 1990; Montalbán et al. 2013). The remarkably regular structure is illustrated on Fig. IV.2.3: oscillations with the same radial orders and angular degrees show clear ridges.

The concept of universal red giant oscillation pattern was introduced by Mosser et al. (2011b), as an alternative form to the usual asymptotic expansion (Tassoul 1980). The second-order asymptotic expansion expresses, for low angular degree ($\ell \ll n$) modes observed around ν_{max} , as

$$\nu_{n,\ell} = \left(n + \varepsilon_{\text{obs}}(\Delta\nu_{\text{obs}}) + d_{0\ell}(\Delta\nu_{\text{obs}}) + \frac{\alpha}{2}(n - n_{\text{max}})^2 \right) \Delta\nu_{\text{obs}}, \quad (1)$$

where the dimensionless parameter n_{max} is defined by $\nu_{\text{max}}/\Delta\nu_{\text{obs}} - \varepsilon_{\text{obs}}$. The observed large separation $\Delta\nu_{\text{obs}}$ and the frequency of maximum oscillation signal ν_{max} are the only free parameters. The radial offset ε_{obs} helps locating the radial ridge; the non-radial offsets $d_{0\ell}$ express the shifts of the different degrees ℓ compared to the radial modes; the second-order term α depends on n_{max} (Mosser et al. 2013b). The quadratic form of Eq. (1) differs from the usual asymptotic expansion since it is based on the large separation $\Delta\nu_{\text{obs}}$ observed at ν_{max} . Hence, $\Delta\nu_{\text{obs}}$ differs from the asymptotic value $\Delta\nu_{\text{as}}$ which should, but cannot, be measured at very high frequency. The relationship between the observed and asymptotic values of the large separation is discussed in Mosser et al. (2013b).

The power of Eq. (1) is shown on Fig. IV.2.4. The clear identification of the ridges, each one corresponding to a given radial order n and angular degree ℓ , demonstrates the universality of the oscillation pattern. With

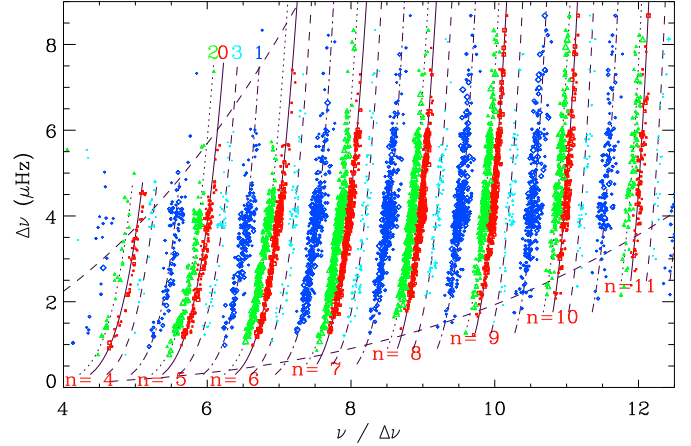


Fig. IV.2.4. Identification of the oscillation modes reported in Fig. IV.2.3, with radial modes in red, dipole modes in dark blue, $\ell = 2$ modes in green, $\ell = 3$ modes in light blue. The solid grey lines superimposed on the ridges indicate the fits of ε for each radial order n . The fits of d_{01} , d_{02} and d_{03} are superimposed on the respective ridges (respectively dash-dot, dot, and dash lines for $\ell = 1, 2$, and 3). The dark dashed lines, derived from the scaling relation dealing with the oscillation excess power, delineate the region where the modes have noticeable amplitudes. Figure from Mosser et al. (2011b) © A&A.

Kepler, the scaling properties were extended at larger $\Delta\nu$ by Corsaro et al. (2012) and at lower $\Delta\nu$ by Mosser et al. (2013a).

2.2.4. Global seismic parameters and evolutionary stages

The measurement of the global seismic parameters carries a rich information. For instance, histograms of the seismic parameters clearly emphasize the red clump and helps identifying the secondary clump stars, massive enough for having ignited helium in non-degenerate conditions (Girardi 1999). The comparison between observed and simulated populations, first performed by Miglio et al. (2009), based on the CoRoT data (Hekker et al. 2009), is discussed in Sect. 3.

A further global seismic parameter is derived from the period spacing of dipole modes. In subgiants and red giants with a radiative core, dipole modes are not pure pressure modes but show a mixed character; they result from the coupling of sound waves in the envelope and gravity waves in the radiative inner region. The period spacing varies with ν^{-2} and also depends on the nature of the mixed mode. It is close to the asymptotic period spacing ($\sqrt{2}\pi^2/\int N_{\text{BV}} d \ln r$ for dipole modes) for gravity-dominated mixed modes, but much below for pressure-dominated mixed modes. Mixed modes in CoRoT red giants were identified by Mosser et al. (2011a). Regardless modelling, period spacings help distinguishing the evolutionary stages of red giants, with significant population differences in the different fields observed by CoRoT. This work opened the way for identifying the asymptotic period spacings in Kepler data (Mosser et al. 2012c), measuring the core rotation (Mosser et al. 2012b), and tracing seismic evolutionary tracks (Mosser et al. 2014).

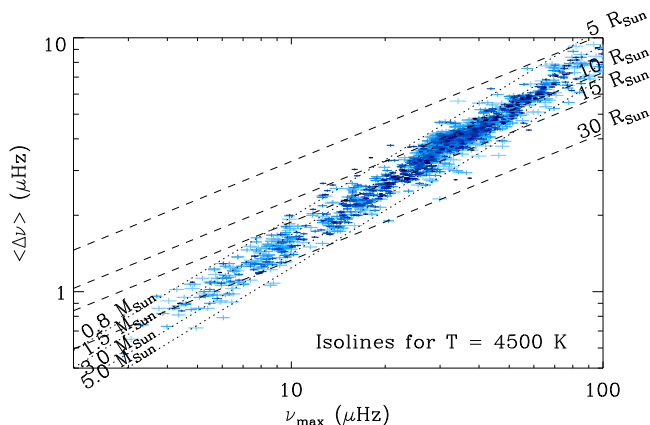


Fig. IV.2.5. ν_{\max} - $\langle\Delta\nu\rangle$ relation for red giants in LRa01 and LRc01. Isoradius and isomass lines, derived from the scalings given by Eqs. (2) and (3), are given for a mean effective temperature of 4500 K. Figure from Mosser et al. (2010) © A&A.

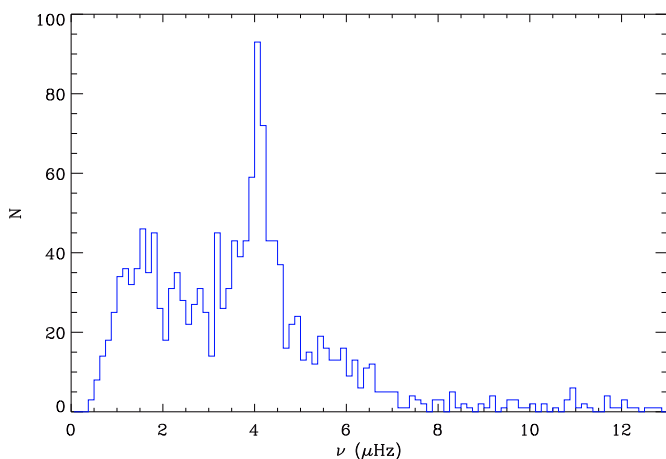


Fig. IV.2.6. Histogram of $\Delta\nu$ of red giants observed during the run LRc01. The peak around 4 μHz is the signature of the red clump. The deficit above 7 μHz is due to the magnitude bias in the detection (Table IV.2.1).

2.3. Scaling relations and ensemble asteroseismology

2.3.1. Light curves and detection

Light curves with a new treatment were recently delivered. The full comparison of the different pipelines providing the global seismic parameters is ongoing. Here, we derive information from the envelope autocorrelation function of the time series (Mosser & Appourchaux 2009) and compare the new data of the LRc01 to the treatment conducted by Mosser et al. (2010). All light curves of the first long run LRc01 were considered, not only those with color indices presumably corresponding to red giants. This allows us to treat all possible red giants, regardless any problems in any prior classification of targets.

The distribution of the large separation is shown on Fig. IV.2.6. The new treatment allows us to enlarge the frequency range where oscillations are detected, with large separations in the interval [0.5–12.5 μHz]. Previous studies were limited within the range [0.75–9.5 μHz]. This new

Table IV.2.1. Distribution of the detection as a function of magnitude. \mathcal{N}_1 is the number of available light curves and \mathcal{N}_2 is the number of red giants showing solar-like oscillations.

Magnitude interval	\mathcal{N}_1	\mathcal{N}_2	$\mathcal{N}_2/\mathcal{N}_1$ %	$(\Delta\nu)_{\text{lim}}$ μHz
11	12	99	43.4	12.1
12	13	735	49.6	11.8
13	14	1890	31.0	10.8
14	15	3673	10.8	7.8
15	16	5010	1.9	5.4
total	11 407	1487		

interval approximately corresponds to stellar radii in the interval [5–35 R_\odot]. Table IV.2.1 shows how the detection depends on the stellar magnitude. Unsurprisingly, the dimmer the magnitude, the more rare the reliable detection of solar-like oscillations. It also emphasizes a bias inherent to the properties of the seismic signal: at dim magnitudes, the global seismic parameters can be detected only for evolved red giants, according to the scaling relation that governs the oscillation amplitude (Mosser et al. 2012a). Table IV.2.1 indicates the limit value $(\Delta\nu)_{\text{lim}}$, corresponding to the typical maximum large separation that can be measured as a function of the visible magnitude. Determining the evolutionary status of these stars is also crucial for forthcoming Galactic archeology analysis (Sect. 3): we could do this for about 25% of the red giants showing solar-like oscillations. The complete study and comparison of all fields observed by CoRoT is in progress (de Assis Peralta et al., in prep.).

2.3.2. Seismic masses and radii

Kallinger et al. (2010) have studied in detail a subsample of faint giant stars obtained in the faint field of CoRoT. Having modelled the convective background noise and the oscillation power excess, they deduced estimates for the stellar mass and radius. Indeed, the importance of the seismic parameters $\Delta\nu_{\text{obs}}$ and ν_{\max} is emphasized by their ability to provide relevant estimates of the stellar mass and radius, since they are respectively related to the square root of the mean density and to the acoustic cutoff frequency, hence to surface gravity, of the stars (Brown et al. 1991):

$$\frac{R}{R_\odot} \simeq \left(\frac{\nu_{\max}}{\nu_{\max,\odot}} \right) \left(\frac{\Delta\nu}{\Delta\nu_\odot} \right)^{-2} \left(\frac{T_{\text{eff}}}{T_\odot} \right)^{1/2}, \quad (2)$$

$$\frac{M}{M_\odot} \simeq \left(\frac{\nu_{\max}}{\nu_{\max,\odot}} \right)^3 \left(\frac{\Delta\nu}{\Delta\nu_\odot} \right)^{-4} \left(\frac{T_{\text{eff}}}{T_\odot} \right)^{3/2}. \quad (3)$$

Mainly empirical, these relations prove to be operant throughout many evolutionary stages (e.g., White et al. 2011a; Belkacem et al. 2013).

However, the calibration of the seismic scaling relations remains an issue. Different works have shown that the extrapolation from the Sun to evolved stars induces small biases and provides too high masses for red giants (e.g., Miglio et al. 2012a; Epstein et al. 2014). We may notice that the very first papers to use the scaling relations, Kallinger et al. (2010) and Mosser et al. (2010), provided an external calibration that reduced the seismic mass. However, this correction has been omitted by further work.

It is also clear that the calibration process of the scaling relations requires precise steps. One of this step is out of reach actually: the determination of ν_{\max} is purely phenomenological and lacks a precise theoretical definition. However, the theoretical approach based on 3D-atmospheric models carried out by Belkacem et al. (2013) indicates that ν_{\max} scales with the acoustic cut-off frequency and the Mach number as $\nu_c \mathcal{M}^3$ (see also Belkacem et al. 2011); this provides strong clues for the relevance of the relation $\nu_{\max} \propto \nu_c$ since \mathcal{M} only shows small variation with stellar evolution. Observationally, the agreement between the spectroscopic measurement of $\log g$ and ν_{\max} (e.g., Pinsonneault et al. 2014) provides us with a good argument about the relevant use of ν_{\max} .

The large separation is a better defined parameter. However, we have too many definitions for it: the large separation we measure at ν_{\max} (e.g., Mosser & Appourchaux 2009) neither corresponds to the asymptotic definition linked to twice the acoustic radius, nor to the dynamical frequency ν_0 that scales as $\sqrt{GM/R^3}$. Even if $\Delta\nu_{\text{obs}}$ provides an acceptable proxy of the dynamical frequency ν_0 , the relationships between these parameters must be investigated in order to accurately calibrate Eqs. (2) and (3) and make the best of the high-quality seismic data (Belkacem et al. 2013).

2.3.3. Stellar evolution

As noted by Stello et al. (2009) on the basis of ground-based and CoRoT observations, the frequencies ν_{\max} and $\Delta\nu$ are closely linked together. They measured $\Delta\nu \propto \nu_{\max}^{0.772 \pm 0.005}$. This relation, derived from the empirical scaling relations defining $\Delta\nu$ and ν_{\max} , was interpreted as the signature of solar-like oscillations. It is now expanded up to the upper red and asymptotic giant branches, where solar-like oscillations correspond to semi-regular variability (Mosser et al. 2013a). From Eqs. (2) and (3), the scaling between ν_{\max} and $\Delta\nu_{\text{obs}}$ expresses

$$\Delta\nu_{\text{obs}} \simeq \nu_0 \propto M^{-1/4} T_{\text{eff}}^{3/8} \nu_{\max}^{3/4}. \quad (4)$$

On the main sequence, the frequency $\Delta\nu_{\text{obs}}$ scales as $\nu_{\max}^{0.8}$ (Verner et al. 2011). The discrepancy between this exponent and the 3/4 value in Eq. (4) is due to the fact that low-mass and high-mass evolution tracks evolve in different regions of the main sequence. On the contrary, the observed scaling exponent on the RGB is closer to 3/4 (Fig. IV.2.5) since the RGB is drawn by the evolution of low-mass stars. Stars with a mass in the range 0.9–1.8 M_{\odot} are present at all stages of the RGB, hence for all ν_{\max} , so that the stellar mass plays no significant role in Eq. (4).

The validity of Eq. (4) is observed over six decades in frequency in the red giant regime (Fig. 2 of Mosser et al. 2013c). This indicates that we can use red giants to track stellar evolution, especially when the information of mixed modes is used (Fig. IV.2.7).

2.3.4. Mode lifetimes and amplitudes

Predicting oscillation amplitudes involves non-adiabatic physics and is much more complex than computing

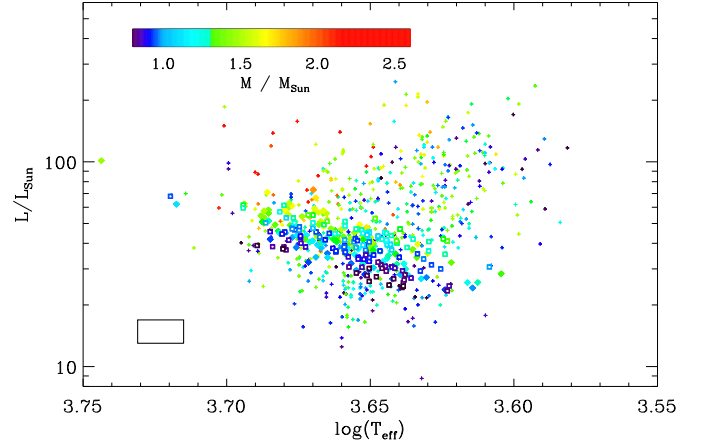


Fig. IV.2.7. HR diagram of the targets with best SNR ratios of LRA01 and LRC01, © A&A, 532, A86. Masses are estimated from the seismic scaling relations. For clarity, individual bars are not represented. Cross are replaced by open squares for red-clump stars and diamonds for secondary-clump stars. The mean 1σ error box is given in the lower-left corner of the diagram.

eigenfrequencies. Amplitudes depend on a balance between mode driving (also referred to as excitation rate) and mode damping (which is proportional to the mode linewidth). Simulations of the excitation are based on 3-D modelling of the upper stellar envelope (Samadi et al. 2015, for a review). Large efforts in this direction are currently made, since such simulations can also be used to address the surface-effect correction due to non-adiabatic effects (Sonoit et al. 2015). Excitation rates of solar-like oscillations across the HR diagram were predicted by Samadi et al. (2007). Assuming adiabatic pulsations, they computed the mode amplitude in terms of surface velocity, converted them into intensity fluctuations, and found that the energy supply rate scales as $(L/M)^{2.6}$ for both main-sequence and red giant stars. The scaling based on the adiabatic intensity-velocity scaling relation results in an under-estimation by a factor of about 2.5 with respect to the CoRoT seismic measurements; this factor is reduced to 1.4 when using non-adiabatic velocity-intensity conversion factors.

These theoretical expectations can be confronted to observations. The scaling of the mode amplitudes with mass and luminosity derived from ensemble asteroseismology shows a more complex dependence than L/M . As an important result, one should note that the ratio between the energy put into the granulation and into the oscillations does not vary with evolution: the ratio H_{\max}/B_{\max} hardly depends on ν_{\max} (H_{\max} and B_{\max} are respectively the mean heights of the oscillations and of the background at ν_{\max} (Mosser et al. 2010; Mathur et al. 2011; Mosser et al. 2012a)).

Amplitudes of radial modes in red giants were also investigated by a detailed analysis of oscillation spectra (i.e. measurements of individual mode heights and mode linewidths) for several hundreds of CoRoT red giants (Baudin et al. 2011). Line widths are small, of about a few tenths of a μHz ; their scaling with T_{eff} shows no important variation, contrary to main-sequence stars. In contrast, Belkacem et al. (2012) theoretically exhibited a scaling as a power law with a large exponent of 10.8. Alternatively,

Corsaro et al. (2012) proposed a scaling varying exponentially with T_{eff} , valid from the main sequence to the red giant domain. Their measurements, based on *Kepler* data, benefit from longer observations: measuring lifetimes requires in fact that modes are resolved, with a duration at least 10 times larger (Appourchaux & Grundahl 2015). So, even *Kepler* data are limited for measuring oscillation lifetimes of evolved red giants radial modes, so that this point remains an issue.

For long-lived dipole mixed modes, the situation is more complex than for radial modes, but Dupret et al. (2009) and Grosjean et al. (2014) could provide the lifetimes of radial and non-radial mixed modes with a time-dependent treatment of convection, for high-mass and low-mass red giants, respectively.

2.3.5. Helium ionization zones

Miglio et al. (2010) found evidence for a periodic component in the oscillation frequencies of in HD 181907 (HR 7349) analyzed by Carrier et al. (2010). As for less-evolved stars (Sect. 3, Part V, Chap 1), the modulation was interpreted as the seismic signature of a sharp structure variation caused by a local depression of the sound speed that occurs in the helium second-ionization region. Such a signature was also observed in a larger set of CoRoT data, but not studied in detail (Fig. 6 of Mosser et al. 2010). It appears at all evolutionary stages, since it is also clearly present in the luminous high-mass red giant studied and in detail by Baudin et al. (2012). Recently, with a large survey of *Kepler* red giants, Vrard et al. (2015) showed that RGB and red clump stars have distinct signatures that can be used to derive the location of the helium second-ionization region but are not precise enough to derive the helium mass fraction.

2.3.6. Rotation

Probing the stellar rotation with seismology requires long-duration observation, unfortunately out of reach with CoRoT. Experience gained with *Kepler* stars shows that more than one year of observation is necessary to detect the core rotation period, typically between 10 and 30 days, in a red giant starting to ascend the RGB, and more than two years for measuring it for red clump stars (e.g., Mosser et al. 2012b; Deheuvels et al. 2014). This limitation is not only a question of frequency resolution; it relies in fact on the detection of gravity dominated mixed modes, whose lifetimes is year long.

Even if undetectable, rotation plays a significant role in red giants, as shown by modelling (Lagarde et al. 2015). Seismic data are now so precise that making the best of them requires the introduction of rotation in the models. Furthermore, Belkacem et al. (2015b,a) showed the intricacy of oscillation and rotation. They developed a formalism that provides a modelling of the wave fluxes in both the mean angular momentum and the mean energy equation. This proves that mixed modes extract angular momentum from the innermost regions of subgiants and red giant, and are a promising candidate to explain the observed spin-down of the core of evolved red giants.

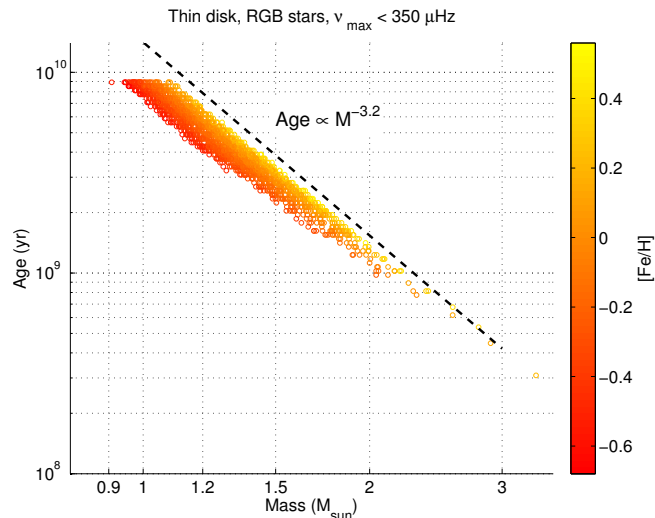


Fig. IV.2.8. Age-mass-metallicity relation for red giants in a TRILEGAL (Girardi et al. 2005) synthetic population representative of thin-disc stars. From Davies & Miglio (2016).

3. Asteroseismology of stellar populations in the Milky Way (by A. Miglio)

Once data from the first CoRoT observational run had been analysed, and solar-like oscillations had been detected in thousands of red giant stars (Hekker et al. 2009), it became clear that the newly available observational constraints $\Delta\nu$ and ν_{max} would allow novel approaches to the study of Galactic stellar populations. Miglio et al. (2009) presented a first comparison between observed and predicted seismic properties of giants in the first CoRoT field, which highlighted the expected signatures of red-clump stars in both distributions.

As described in Sect. 2, average seismic parameters may be combined with estimates of surface temperature to infer radii and masses for all stars with detected oscillations. A step forward in studies of stellar populations with seismic constraints was then taken when empirical and/or theoretical support for the seismically inferred masses and radii became available (Belkacem et al. 2011; White et al. 2011b; Miglio et al. 2012a; Miglio 2012; Miglio et al. 2013a; Belkacem et al. 2013).

First, it was soon realised that solar-like oscillating red giants may be used as accurate distance indicators probing regions out to about 10 kpc: as in the case of eclipsing binaries the distance to each red giant may be estimated from the absolute luminosity, which is obtained from the asteroseismically determined radius and T_{eff} . Giants observed by CoRoT may be used as distance indicators, crucially mapping regions at different Galactocentric radii (Miglio et al. 2012b, 2013b).

Second, and foremost, seismically determined masses of RGB stars make it possible to estimate the ages of thousands field stars. The age of low-mass red-giant stars is largely determined by the time spent on the main sequence, hence by the initial mass of the red giant's progenitor ($\tau_{\text{MS}} \propto M/L(M) \propto M_{\text{ini}}^{-(\nu-1)}$ with $\nu = 3-5$, e.g. see Kippenhahn et al. 2012 and Fig. IV.2.8). Solar-like oscillating giants cover a mass range from $\simeq 0.9$ to $\simeq 3 M_{\odot}$, which

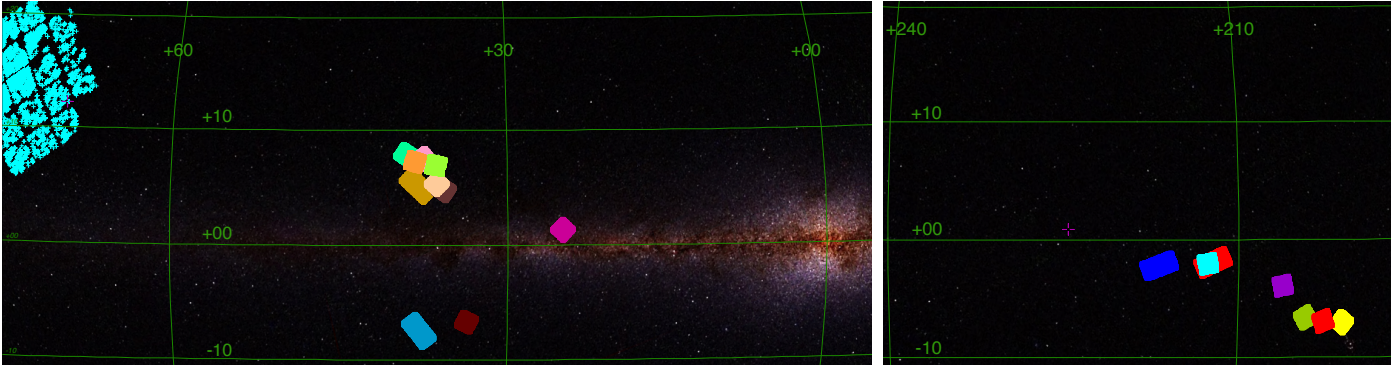


Fig. IV.2.9. Position in galactic coordinates of stars observed by CoRoT in the centre (*left panel*) and antcentre (*right panel*) fields. The *Kepler* field of view is also shown in the top-left corner of the left panel. This figure was made using the Aladin Sky Atlas (Bonnarel et al. 2000), and the background image is based on the 2MASS catalogue (Skrutskie et al. 2006).

in turn maps to an age range spanning $\simeq 0.3$ to $\simeq 12$ Gyr, i.e., the entire Galactic history.

A first example of Galactic archeology utilising asteroseismic constraints is the differential population study presented in Miglio et al. (2013b). On the basis of comparisons with synthetic stellar populations, the authors interpreted the differences in the mass distributions as being due mainly to the different average heights of the observed fields below the galactic plane. Since it is believed that dynamical processes in the disc increase the velocity dispersion of stars with time, it follows that older stellar populations reach greater heights above and below the plane. Other data had already hinted at a similar dependence, as for instance an increase of the velocity dispersion of stars with increasing age (Holmberg et al. 2009), or the correlation between scale height and $[O/Fe]$ (Bovy et al. 2012), but they were only available for stars in the immediate solar vicinity.

While these first results demonstrated the potential of solar-like oscillating K giants as probes of the Milky Way’s structure and evolution, significant steps forward are now being taken and this approach is being significantly refined and extended. Spectroscopic constraints have now become available for and are adding crucial constraints on age-velocity and age-metallicity relations as well (see Sect. 3.2). Moreover, it is now possible to extend these studies to stars probing the Galaxy at different heights from the plane and at different Galactocentric radii by considering data collected by *Kepler*, K2 (Howell et al. 2014), and by harvesting data from the numerous fields that CoRoT has observed (see Fig. IV.2.9).

3.1. Data available

Only two CoRoT long-observational runs have been analysed so far (Hekker et al. 2009; Mosser et al. 2011a; Miglio et al. 2013b). Data collected in 15 additional runs, crucially exploring stellar populations at different galactocentric radii, are yet to be exploited. Figure IV.2.10 shows the number of stars targeted in CoRoT’s observational campaigns in the colour-magnitude range expected to be populated by red giants with detectable oscillations. The analysis of these data is currently ongoing, and complement the observations by K2 (Howell et al. 2014), which will also map several regions of the Milky Way, although with data of shorter duration (~ 80 d).

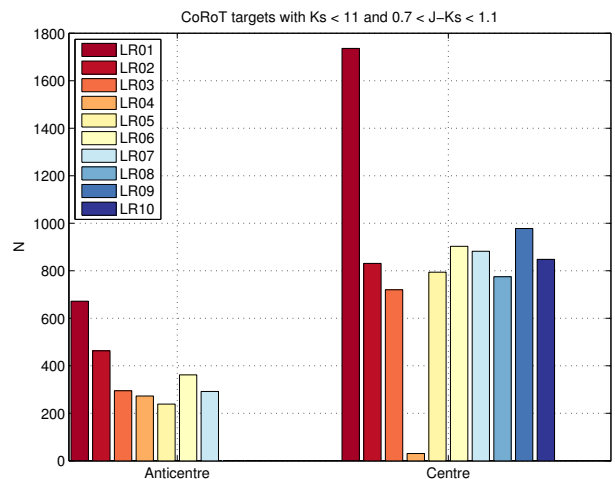


Fig. IV.2.10. Number of stars observed in CoRoT’s exofields in the colour-magnitude range expected to be populated by red giants with detectable oscillations ($0.7 < J - K_s < 1.1$, $K_s < 11$). The analysis of the first two observational runs led to the detection of oscillations in about 1600 (LRc01) and 400 (LRa01) stars, as reported in Hekker et al. (2009) and Mosser et al. (2010). The varying number of stars per field reflects different target selection functions used, the failure of 2 CCD modules, as well as the different stellar density in each field.

Moreover, in the last few observing runs of CoRoT, thanks to the coordination between the asteroseismology and exoplanet thematic teams, it was possible to define a target selection function which can be easily taken into account when comparing with synthetic populations. As an example we report here the selection criteria adopted for LRc09. By comparison with expected populations (see Fig. IV.2.11) a colour cut $0.7 \leq J - K \leq 1.2$ was adopted to minimise contamination by red dwarfs. Such a target selection function will allow robust comparisons against synthetic populations, and is simpler to account for compared to that of the nominal *Kepler* mission (Farmer et al. 2013) and of the first CoRoT fields (Miglio et al. 2013a).

3.2. Synergies with spectroscopic surveys

Since the CoRoT asteroseismic data provide a very accurate ($\sigma_{\log g} \sim 0.05$ dex) way to determine surface gravities

(e.g., see Bruntt et al. 2010; Morel & Miglio 2012; Creevey et al. 2013), they can also play an important rôle in helping to calibrate spectroscopic analyses. This prompted the establishment of formal collaborations between CoRoT and large spectroscopic surveys, such as APOGEE (Majewski et al. 2010), the Gaia ESO Public Spectroscopic Survey (Gilmore et al. 2012), and GALAH (De Silva et al. 2015).

On top of increasing the precision and accuracy of spectroscopic analyses (e.g. see Morel 2015), the combination of asteroseismic and spectroscopic observations opens the possibility to combine accurate ages of tens of thousands of stars with constraints on kinematics and on chemical abundances and build chemodynamical maps as a function of age in various regions of the Galaxy. This will be used to quantify, by comparison with predictions of chemodynamical models of the Galaxy, the relative importance of various processes which play a rôle in shaping the Milky Way, for example in-situ star formation, mergers, and dynamical processes such as diffusion and migration of stars (e.g. see Freeman & Bland-Hawthorn 2002; Chiappini et al. 2015).

Work has only recently started on combining spectroscopic and seismic constraints. A first surprising result from the CoRoT & APOGEE collaboration (CoRoGEE) was reported in Chiappini et al. (2015). The authors detected stars rich in alpha elements which appear to be massive, hence likely to be young stars. This finding has potentially ground-breaking implications on the widely accepted use of $[\alpha/\text{Fe}]$ as a proxy for age. Interestingly, the CoRoT data seem to suggest a higher fraction of these stars in the inner Galaxy, providing a clue to explain their origin. Stars with similar, unexpected, properties were also found among K giants observed by Kepler and APOGEE (Martig et al. 2015).

A first comprehensive work based on exploiting the combination of asteroseismic and spectroscopic constraints is presented in Anders (2016). This work made use of CoRoGEE stars in LRC01 and LRA01 and enabled, for the first time, studies of the $[\alpha/\text{Fe}]-[\text{Fe}/\text{H}]$ -age relation outside the Solar vicinity. Even with this first, small sample of stars, it was possible to place robust constraints on the chemical evolution of the Milky Way's stellar disc, finding, for instance, strong signatures of inside-out formation of the Galactic disc (Chiappini et al. 1997). Also, when comparing these findings to chemical-evolution models, some interesting discrepancies appeared, such as the existence of super-metal-rich stars, and the exact shape of the $[\alpha/\text{Fe}]-[\text{Fe}/\text{H}]$ distribution in the inner regions of the disc, suggesting that a significant fraction of stars now observed near the Solar neighbourhood might have migrated from inner regions.

3.3. The rôle of CoRoT

CoRoT has been the pioneer in providing data for studies of the Milky Way using asteroseismic constraints. It has also been instrumental in fostering direct collaborations and discussions between expert researchers in Galactic evolution, specialists in stellar structure, asteroseismology, stellar populations synthesis, and spectroscopists⁴. The discussions that stemmed from the interpretation of CoRoT data, were then expanded into strategies for the coordinated analyses of data from Kepler, and from future space

⁴ see e.g. <http://www.asterostep.eu/>

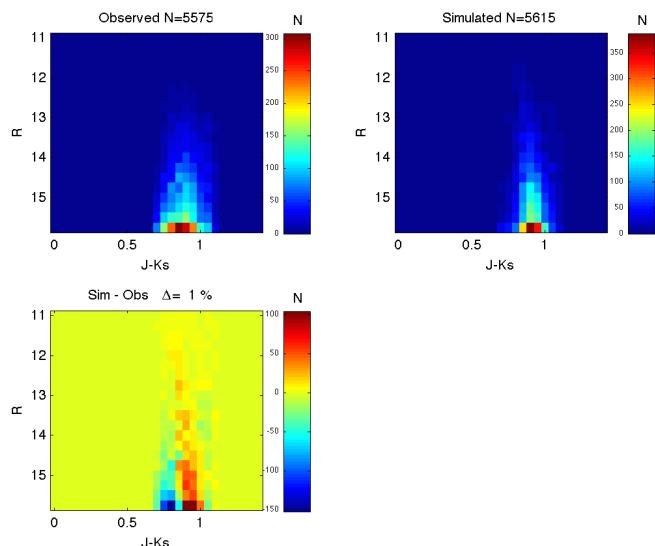


Fig. IV.2.11. Star counts in colour-magnitude bins for all stars in the FOV and in TRILEGAL (Girardi et al. 2005; Girardi et al. 2015) synthetic population, assuming reddening at infinity by Drimmel et al. (2003) only for stars selected by a colour-magnitude criterion, $0.7 \leq J-K \leq 1.2$, and here $R < 16$.

missions. For instance, results from CoRoT provided compelling scientific motivation to include Galactic archeology as part of the programme of K2 (Howell et al. 2014), PLATO (Rauer et al. 2014), and TESS (Ricker et al. 2014) missions.

However, rather than relegating CoRoT to the role of pioneer, it is worth recalling that the exploitation of CoRoT data, in particular in combination with chemodynamical constraints, has only just started. The analysis of data in various observing fields (see Figs. IV.2.9 and IV.2.10) will generate ages and chemical abundance patterns of field stars over a large radial range of the Milky Way, adding strong observational evidence to address open questions concerning, e.g., the star formation history in the disc, star aggregates and streams, and quantify effects of radial migration and disc heating (Freeman 2012).

References

- Anders, 2016, A&A, submitted
 Appourchaux, T., & Grundahl, F. 2015, Asteroseismology observations and space missions, eds. V. C. H. Tong, & R. A. Garcia
 Arentoft, T., Kjeldsen, H., Bedding, T. R., et al. 2008, ApJ, 687, 1180
 Auvergne, M., Bodin, P., Boisnard, L., et al. 2009, A&A, 506, 411
 Barban, C., De Ridder, J., Mazumdar, A., et al. 2004, in SOHO 14 Helio- and Asteroseismology: Towards a Golden Future, ed. D. Danesy, ESA SP, 559, 113
 Barban, C., Matthews, J. M., De Ridder, J., et al. 2007, A&A, 468, 1033
 Baudin, F., Barban, C., Belkacem, K., et al. 2011, A&A, 529, A84
 Baudin, F., Barban, C., Goupil, M. J., et al. 2012, A&A, 538, A73

- Bedding, T. R., Kjeldsen, H., Campante, T. L., et al. 2010, *ApJ*, 713, 935
- Belkacem, K., Goupil, M. J., Dupret, M. A., et al. 2011, *A&A*, 530, A142
- Belkacem, K., Dupret, M. A., Baudin, F., et al. 2012, *A&A*, 540, L7
- Belkacem, K., Samadi, R., Mosser, B., Goupil, M.-J., & Ludwig, H.-G. 2013, in *ASP Conf. Ser.* 479, eds. H. Shibahashi, & A. E. Lynas-Gray, 61
- Belkacem, K., Marques, J. P., Goupil, M. J., et al. 2015a, *A&A*, 579, A31
- Belkacem, K., Marques, J. P., Goupil, M. J., et al. 2015b, *A&A*, 579, A30
- Bonnarel, F., Fernique, P., Bienaymé, O., et al. 2000, *A&AS*, 143, 33
- Bovy, J., Rix, H.-W., Hogg, D. W., et al. 2012, *ApJ*, 755, 115
- Brown, T. M., Gilliland, R. L., Noyes, R. W., & Ramsey, L. W. 1991, *ApJ*, 368, 599
- Bruntt, H., Bedding, T. R., Quirion, P.-O., et al. 2010, *MNRAS*, 405, 1907
- Carrier, F., De Ridder, J., Baudin, F., et al. 2010, *A&A*, 509, A73
- Chiappini, C., Matteucci, F., & Gratton, R. 1997, *ApJ*, 477, 765
- Chiappini, C., Anders, F., Rodrigues, T. S., et al. 2015, *A&A*, 576, L12
- Corsaro, E., Stello, D., Huber, D., et al. 2012, *ApJ*, 757, 190
- Creevey, O. L., Thévenin, F., Basu, S., et al. 2013, *MNRAS*, 431, 2419
- Davies, G. R., & Miglio, A. 2016, *Astron. Nachr.*, in press
- De Ridder, J., Barban, C., Carrier, F., et al. 2006, *A&A*, 448, 689
- De Ridder, J., Barban, C., Baudin, F., et al. 2009, *Nature*, 459, 398
- De Silva, G. M., Freeman, K. C., Bland-Hawthorn, J., et al. 2015, *MNRAS*, 449, 2604
- Deheuvels, S., Doğan, G., Goupil, M. J., et al. 2014, *A&A*, 564, A27
- Drimmel, R., Cabrera-Lavers, A., & López-Corrodoira, M. 2003, *A&A*, 409, 205
- Dupret, M.-A., Belkacem, K., Samadi, R., et al. 2009, *A&A*, 506, 57
- Dziembowski, W. A., Gough, D. O., Houdek, G., & Sienkiewicz, R. 2001, *MNRAS*, 328, 601
- Eddington, A. S. 1917, *The Observatory*, 40, 290
- Epstein, C. R., Elsworth, Y. P., Johnson, J. A., et al. 2014, *ApJ*, 785, L28
- Farmer, R., Kolb, U., & Norton, A. J. 2013, *MNRAS*, 433, 1133
- Frandsen, S., Carrier, F., Aerts, C., et al. 2002, *A&A*, 394, L5
- Freeman, K. 2012, in *Red Giants as Probes of the Structure and Evolution of the Milky Way*, eds. A. Miglio, J. Montalbán, & A. Noels, *ApSS Proceedings*
- Freeman, K., & Bland-Hawthorn, J. 2002, *ARA&A*, 40, 487
- Gilliland, R. L., Brown, T. M., Kjeldsen, H., et al. 1993, *AJ*, 106, 2441
- Gilmore, G., Randich, S., Asplund, M., et al. 2012, *The Messenger*, 147, 25
- Girardi, L. 1999, *MNRAS*, 308, 818
- Girardi, L., Groenewegen, M. A. T., Hatziminaoglou, E., & da Costa, L. 2005, *A&A*, 436, 895
- Girardi, L., Barbieri, M., Miglio, A., et al. 2015, *Astrophys. Space Sci. Proc.*, 39, 125
- Grosjean, M., Dupret, M.-A., Belkacem, K., et al. 2014, *A&A*, 572, A11
- Hekker, S., Aerts, C., De Ridder, J., & Carrier, F. 2006, *A&A*, 458, 931
- Hekker, S., Kallinger, T., Baudin, F., et al. 2009, *A&A*, 506, 465
- Holmberg, J., Nordström, B., & Andersen, J. 2009, *A&A*, 501, 941
- Howell, S. B., Sobeck, C., Haas, M., et al. 2014, *PASP*, 126, 398
- Kallinger, T., Zwintz, K., Pamyatnykh, A. A., Guenther, D. B., & Weiss, W. W. 2005, *A&A*, 433, 267
- Kallinger, T., Guenther, D. B., Matthews, J. M., et al. 2008a, *A&A*, 478, 497
- Kallinger, T., Guenther, D. B., Weiss, W. W., et al. 2008b, *Communications in Asteroseismology*, 153, 84
- Kallinger, T., Weiss, W. W., Barban, C., et al. 2010, *A&A*, 509, A77
- Kallinger, T., Matthews, J. M., Guenther, D. B., et al. 2012, in *Progress in Solar/Stellar Physics with Helio- and Asteroseismology*, eds. H. Shibahashi, M. Takata, & A. E. Lynas-Gray, *ASP Conf. Ser.*, 462, 156
- Kim, K. M., Mkrtychian, D. E., Lee, B.-C., Han, I., & Hatzes, A. P. 2006, *A&A*, 454, 839
- Kippenhahn, R., & Weigert, A. 1990, *Stellar Structure and Evolution*
- Kippenhahn, R., Weigert, A., & Weiss, A. 2012, *Stellar Structure and Evolution*
- Kjeldsen, H., & Bedding, T. R. 1995, *A&A*, 293, 87
- Lagarde, N., Miglio, A., Eggenberger, P., et al. 2015, *ArXiv e-prints*
- Lebreton, Y., & Goupil, M. J. 2014, *A&A*, 569, A21
- Majewski, S. R., Wilson, J. C., Hearty, F., Schiavon, R. R., & Skrutskie, M. F. 2010, in *IAU Symp.* 265, eds. K. Cunha, M. Spite, & B. Barbuy, 480
- Martig, M., Rix, H.-W., Aguirre, V. S., et al. 2015, *MNRAS*, 451, 2230
- Mathur, S., Hekker, S., Trampedach, R., et al. 2011, *ApJ*, 741, 119
- Mazumdar, A., Mérand, A., Demarque, P., et al. 2009, *A&A*, 503, 521
- Miglio, A. 2012, *Asteroseismology of Red Giants as a Tool for Studying Stellar Populations: First Steps*, eds. A. Miglio, J. Montalbán, & A. Noels, 11
- Miglio, A., Montalbán, J., Baudin, F., et al. 2009, *A&A*, 503, L21
- Miglio, A., Montalbán, J., Carrier, F., et al. 2010, *A&A*, 520, L6
- Miglio, A., Brogaard, K., Stello, D., et al. 2012a, *MNRAS*, 419, 2077
- Miglio, A., Morel, T., Barbieri, M., et al. 2012b, in *Eur. Phys. J. Web Conf.*, 19, 5012
- Miglio, A., Chiappini, C., Morel, T., et al. 2013a, in *Eur. Phys. J. Web Conf.*, 43, 3004
- Miglio, A., Chiappini, C., Morel, T., et al. 2013b, *MNRAS*, 429, 423
- Montalbán, J., Miglio, A., Noels, A., et al. 2013, *ApJ*, 766, 118
- Morel, T. 2015, *Astrophys. Space Sci. Proc.*, 39, 73

- Morel, T., & Miglio, A. 2012, *MNRAS*, 419, L34
- Mosser, B., & Appourchaux, T. 2009, *A&A*, 508, 877
- Mosser, B., Belkacem, K., Goupil, M., et al. 2010, *A&A*, 517, A22
- Mosser, B., Barban, C., Montalbán, J., et al. 2011a, *A&A*, 532, A86
- Mosser, B., Belkacem, K., Goupil, M., et al. 2011b, *A&A*, 525, L9
- Mosser, B., Elsworth, Y., Hekker, S., et al. 2012a, *A&A*, 537, A30
- Mosser, B., Goupil, M. J., Belkacem, K., et al. 2012b, *A&A*, 548, A10
- Mosser, B., Goupil, M. J., Belkacem, K., et al. 2012c, *A&A*, 540, A143
- Mosser, B., Dziembowski, W. A., Belkacem, K., et al. 2013a, *A&A*, 559, A137
- Mosser, B., Michel, E., Belkacem, K., et al. 2013b, *A&A*, 550, A126
- Mosser, B., Samadi, R., & Belkacem, K. 2013c, in *SF2A-2013: Proceedings of the Annual meeting of the French Society of Astronomy and Astrophysics*, eds. L. Cambresy, F. Martins, E. Nuss, & A. Palacios, 25
- Mosser, B., Benomar, O., Belkacem, K., et al. 2014, *A&A*, 572, L5
- Pinsonneault, M. H., Elsworth, Y., Epstein, C., et al. 2014, *ApJS*, 215, 19
- Rauer, H., Catala, C., Aerts, C., et al. 2014, *Exper. Astron.*, 38, 249
- Retter, A., Bedding, T. R., Buzasi, D. L., Kjeldsen, H., & Kiss, L. L. 2003, *ApJ*, 591, L151
- Ricker, G. R., Winn, J. N., Vanderspek, R., et al. 2014, in *SPIE Conf. Ser.*, 9143, 20
- Samadi, R., Georgobiani, D., Trampedach, R., et al. 2007, *A&A*, 463, 297
- Samadi, R., Belkacem, K., Ludwig, H.-G., et al. 2013, *A&A*, 559, A40
- Samadi, R., Belkacem, K., & Sonoi, T. 2015, *ArXiv e-prints*
- Skrutskie, M. F., Cutri, R. M., Stiening, R., et al. 2006, *AJ*, 131, 1163
- Soderblom, D. R. 2010, *ARA&A*, 48, 581
- Sonoi, T., Samadi, R., Belkacem, K., et al. 2015, *A&A*, 583, A112
- Stello, D., Kjeldsen, H., Bedding, T. R., & Buzasi, D. 2006, *A&A*, 448, 709
- Stello, D., Bruntt, H., Kjeldsen, H., et al. 2007, *MNRAS*, 377, 584
- Stello, D., Bruntt, H., Preston, H., & Buzasi, D. 2008, *ApJ*, 674, L53
- Stello, D., Chaplin, W. J., Basu, S., Elsworth, Y., & Bedding, T. R. 2009, *MNRAS*, 400, L80
- Tarrant, N. J., Chaplin, W. J., Elsworth, Y., Sreckley, S. A., & Stevens, I. R. 2007, *MNRAS*, 382, L48
- Tassoul, M. 1980, *ApJS*, 43, 469
- Tong, V., & Garcia, R. 2015, *Extraterrestrial Seismology*, eds. V. C. H. Tong, & R. A. Garcia
- Ulrich, R. K. 1986, *ApJ*, 306, L37
- Verner, G. A., Elsworth, Y., Chaplin, W. J., et al. 2011, *MNRAS*, 415, 3539
- Vrard, M., Mosser, B., Barban, C., et al. 2015, *A&A*, 579, A84
- White, T. R., Bedding, T. R., Stello, D., et al. 2011a, *ApJ*, 742, L3
- White, T. R., Bedding, T. R., Stello, D., et al. 2011b, *ApJ*, 743, 161

Acknowledgements: The CoRoT space mission has been developed and operated by CNES, with the contribution of Austria, Belgium, Brazil, ESA, Germany, and Spain.